Properties of surface waves determined via bistatic terahertz impulse ranging

M. T. Reiten, D. Grischkowsky, and R. A. Cheville[a)]
School of Electrical and Computer Engineering and Center for Laser and Photonics Research, Oklahoma State University, Stillwater, Oklahoma 74078

(Received 18 April 2000; accepted for publication 18 December 2000)

A bistatic terahertz impulse ranging system has permitted the full isolation and direct measurements of the surface wave loss and dispersion for terahertz frequencies on a dielectric cylinder. This system permits ranging investigations with variable bistatic angles between the source and detector. Direct, frequency dependent comparisons of surface wave loss and propagation velocity are compared to Mie theory and previous measurements of surface wave propagation over a 1 THz bandwidth. The observed radiation from the surface waves is seen to depend on the path of the radiation in and along the scatterer. © *2001 American Institute of Physics.*
[DOI: 10.1063/1.1350418]

Since the early work of Clebsch and Mie[1] analytic solutions for electromagnetic scattering have been approached in the frequency domain by solving for fields at boundaries. Although analytical solutions or approximations are possible for geometrically simple objects, frequency domain approaches are not physically transparent because the contributions from various scattering mechanisms are entangled together in the mathematical analysis. The extraction of the physics of scattering mechanisms from the boundary value solution has been a problem of long-term interest.[2,3]

An alternative method of extracting the physical mechanisms of scattering is to localize the excitation energy through use of a short duration pulse. Here instead of directly measuring frequency resonances, a short pulse in time with a corresponding broad spectrum is used. This temporal resolution permits the experimental isolation of processes in time which are difficult to extract from boundary value methods such as propagation of surface waves[4] and Gouy phase shifts.[5] The contributions of various physical mechanisms to the total scattered field depend strongly on geometry-dominant mechanisms.

We report the direct measurement of the frequency dependent propagation of surface waves in the THz frequency regime over a range of angles. The complex index of refraction obtained through physical optics analysis compared with previous results demonstrates enhancement of surface wave contributions for angles near backscattering.

The impulse ranging system reported here and shown in Fig. 1(a), is a modification of the fixed bistatic THz impulse ranging system.[6] This system utilizes picosecond electromagnetic pulses to illuminate the target with a time gated, coherent measurement of the scattered field over a 1 THz bandwidth. The angle θ between the source and the detector can be adjusted from 21° to 180° about the axis of rotation as defined by the location of the target.

An optoelectronically generated THz pulse is created with a coplanar stripline structure on a GaAs substrate biased at 90 V_{dc} using focused laser pulses (50 fs, 820 nm center wavelength, 80 MHz repetition rate). The THz beam is then collimated by a paraboloidal reflector with focal length f = 119 mm. A planar deflection mirror placed 75 mm from the paraboloidal reflector steers the THz beam. The cylindri-

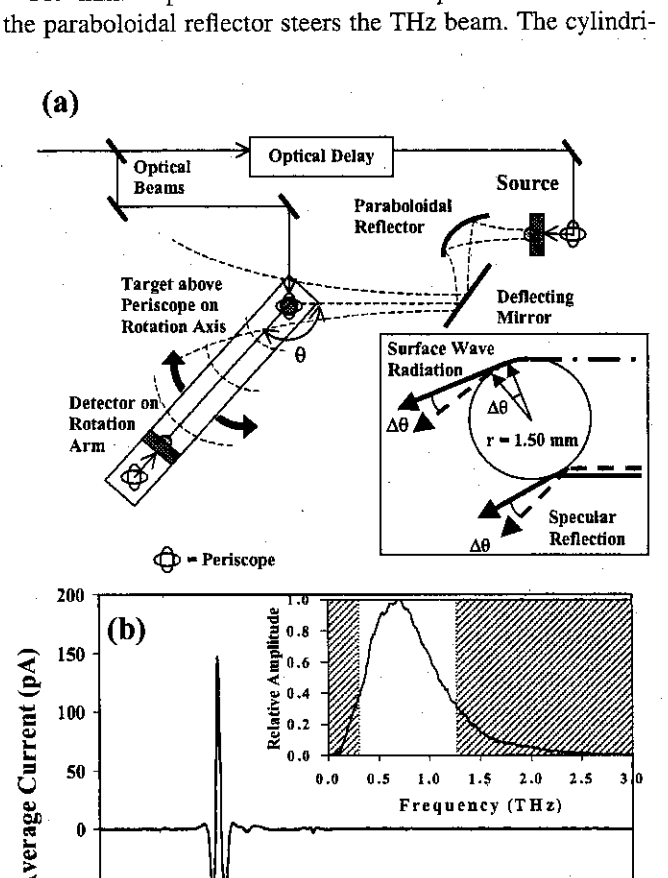

FIG. 1. (a) Diagram of variable angle THz impulse radar range. The target, periscope beneath the target and the detector rotation arm all share the same axis of rotation. (b) Signal measurement at θ=180° without a target with the associated spectrum shown in the inset. The unshaded region corresponds to the valid spectral range of the surface wave reference spectrum measured at θ=150°.

a)Electronic mail: kridnix@okstate.edu

cal target is placed 400 mm from the deflection mirror and above the axis point for the rotating receiver arm. No subsequent focusing lens[7] was used since the diameter of the beam at the target is 16.4 mm at the maximum frequency of 1.3 THz, leading to a negligible phase shift across the target. Scattered THz radiation is then detected by the receiver antenna with an 8 mm diameter aperture placed 265 mm from the target. The 8 mm aperture corresponds to a phase front curvature at the receiver of less than $\lambda/30$ at the central wavelength and defines an angular resolution of 1.5°. A silicon lens focuses the THz radiation onto the receiving antenna, a 30 μm dipole. The THz beam is modulated at 383 Hz and a current amplifier and a lock-in amplifier detect the current. The absolute timing between the optical pulses in this free space system is maintained between different measurement angles θ by steering the detector gating beam along the rotation arm axis with a periscope beneath the target, shown in Fig. 1(a). The periscope has one mirror fixed with respect to the incoming optical beam while the second mirror rotates with the rotation arm. The optical beam at the detector does not walk off the 5 μm antenna gap or shift in time more than 10 fs over a range of 60°.

The measured THz impulse waveform and associated spectrum, shown in Fig. 1(b), establish an absolute time reference. The valid spectral range for the surface wave measurements are between 0.3 and 1.3 THz (shown by the unshaded areas) determined by the signal-to-noise ratio of the surface wave reference spectrum, E_{ref}. The target used for these measurements is a high dimensional accuracy alumina rod with radius, $r=1.500\pm0.001$ mm. The incident electric field is oriented perpendicularly to the axis of the cylinder (TE configuration). The alumina cylinder target has a measured index of refraction of $n=3.17$.[8]

The time dependent scattered electric field is shown in Fig. 2(a) on the same absolute time scale as in Fig. 1(b). As in previous THz impulse measurements, temporally isolated scattering mechanisms are clearly visible; a specular reflection striking the surface of the cylinder at glancing incidence (S), the surface or creeping wave radiation (Θ), and a wave propagating through the target (T). The surface wave arises for the portion of the incidence pulse which strikes the cylinder at near grazing incidence [τ_0 in inset of Fig. 2(a)], couples to the surface, and travels around the outside of the target. Due to the curvature of the cylinder this surface wave continually loses power to tangential radiation emission. The absolute time of arrival of the surface wave radiation is measurable because the distance from the tangent of the cylinder [τ_θ in the inset of Fig. 2(a)] to the detector is constant as the rotation arm and the cylindrical target are axially aligned. As all the angular measurements share the same τ_0, the only change in path length for the corresponding surface waves between two angular measurements is the additional propagation distance across the surface.

As expressed in Eq. (1) where $E_{\text{rev}}(\omega,\theta)$ is the signal detected at the receiver, $E_{\text{surf}}(\omega,\theta)$ is the electric field of the surface wave pulse on the target surface, and $R(\omega)$ describes the outcoupling of radiation. The complex and frequency dependent effective index of refraction, n_{eff} is used to determine the wave vector of the surface wave tangent to the surface, $n_{\text{eff}}k_0$, with k_0 the associated free space wave vector.

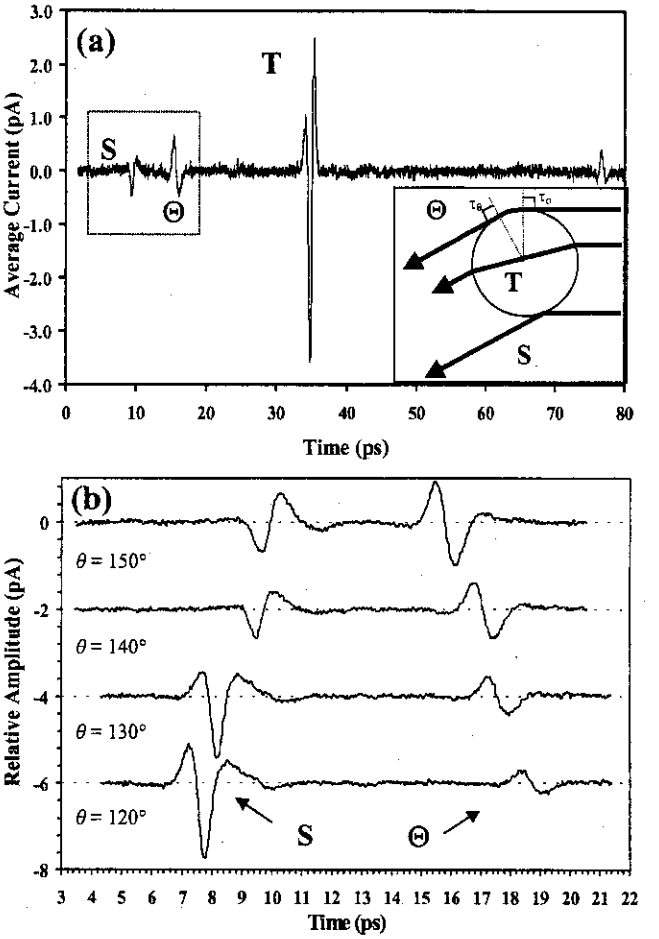

FIG. 2. (a) Typical measured impulse response of 1.50 mm radius alumina cylinder at $\theta=150°$ (four averages). The inset shows τ_0, the incident tangent point, and τ_θ, the tangent point to the detector. (b) Measured specular reflection and surface waves at various θ (16 averages) offset for clarity. Identified features (S) specular reflection, (Θ) surface wave, and (T) transmitted wave.

r is the radius of the cylinder and θ is the angular propagation of the surface wave measured from the point on the cylinder tangent to the wave vector of the incident plane wave:

$$E_{\text{rev}}(\omega,\theta)=R(\omega)E_{\text{surf}}(\omega,\theta)$$
$$=R(\omega)E_{\text{surf}}(\omega,0)e^{-in_{\text{eff}}k_0r\theta}. \quad (1)$$

The leaking of radiation from the surface wave tangentially from the surface into space is responsible for the pulse labeled Θ in Fig. 2. The energy path or Poynting vector of these waves is fundamentally different from surface waves measured previously at more acute angles ($\theta\cong10°$).[8] At small bistatic detection angles ($\theta<36°$ for alumina), the observed surface waves measured takes a path through the dielectric at the critical angle and reemerges further along the surface[7] to travel as a surface wave. Radiation which "cuts through" the cylinder and couples out to a surface wave suffers less loss than that which travels purely on the surface for a given angular distance.

To measure surface wave propagation characteristics we vary θ such that the surface wave travels along path lengths differing by $d_{\text{surf}}=r\Delta\theta$, where r is the radius of the target and $\Delta\theta$ is the change in θ between two measurements as shown in the inset of Fig. 1(a). Measurements over oblique

angles, covering the range $120° \leqslant \theta \leqslant 150°$, permit temporal isolation of the surface wave from the other scattering processes observed in Fig. 2(a). In addition the relative short path length permits observation before the lossy surface wave decays below the signal-to-noise limit of the system. Specular reflection and surface wave measurements are shown in Fig. 2(b) over a range from $\theta = 150°$ to 120° in 10° increments. Absolute timing is preserved between each measurement angle. Changes in the relative amplitudes of the specular (S) and surface wave (Θ) are immediately observable. The changing shape of the leading specular pulse is due to an incrementally larger surface area on the target contributing to reflection and the corresponding phase shift. The decreasing amplitude of the surface wave radiation is due to the loss mechanisms discussed previously.

The subpicosecond temporal resolution of the measurement system permits the Fourier transform of the isolated surface wave pulses to obtain the associated spectra.[4] In order to deconvolve system response, the ratio of the signal spectrum to a reference spectrum, as in Eq. (2), isolates the surface wave behavior independent of coupling mechanisms:

$$\frac{E_{\mathrm{sig}}(\omega,\theta+\Delta\theta)}{E_{\mathrm{ref}}(\omega,\theta)} = \frac{R(\omega)E_{\mathrm{surf}}(\omega,0)e^{-in_{\mathrm{eff}}k_0 r(\theta+\Delta\theta)}}{R(\omega)E_{\mathrm{surf}}(\omega,0)e^{-in_{\mathrm{eff}}k_0 r\theta}} = e^{-in_{\mathrm{eff}}(\omega)k_0 r\Delta\theta} = e^{-ik_{\mathrm{surf}}(\omega)d_{\mathrm{surf}}}. \quad (2)$$

E_{ref} is the reference spectrum which is the isolated surface wave measured at $\theta = 150°$ and E_{sig} are the corresponding signal spectra taken at the signal angles of 140°, 130°, and 120°. The use of a surface wave as the reference spectra permits direct measurement of surface wave propagation since any coupling mechanisms are divided out in Eq. (2); $\Delta\theta$ is the change in angle between the signal and reference spectrum. Note, that this notation is formally equivalent to the notation used in previous measurements[4] describing a wave propagating along a surface path length $d_{\mathrm{surf}} = r\Delta\theta$ with propagation constant $k_{\mathrm{surf}}(\omega) = n_{\mathrm{effs}}(\omega)k_0$.

Figure 3 shows the real part of the effective index, $n(\omega) = \mathrm{Re}(n_{\mathrm{eff}})$, and the field loss coefficient, $\alpha(\omega) = \mathrm{Im}(n_{\mathrm{eff}})k_0$, measured as a function of frequency. The measured values, $n_{\mathrm{meas}}(\omega)$ and $\alpha_{\mathrm{meas}}(\omega)$, are the averaged values from the three angles to reduce noise. The individual measurements at each angle varied by no more than $\pm 10\%$. These results agree well with values generated by Mie theory numerical analysis using parameters matching the experimental configuration. The values for $n_{\mathrm{mie}}(\omega)$ and $\alpha_{\mathrm{mie}}(\omega)$ used for comparison in Fig. 3 were determined following the same procedure outlines above, but numerically determining scattering from the measured reference pulse in Fig. 1(b).

Prior measurements of the surface wave at acute angles with a fixed bistatic geometry yielded values for $n_{\mathrm{eff}} = 1.1 + 0.073i$, but were unable to obtain the frequency dependence and measured surface waves that cut through a chord of the cylinder.[8] The real index in Fig. 3(a) is within 4% of the previously published results in the valid spectral range and closely matches Mie theory predictions. The low value

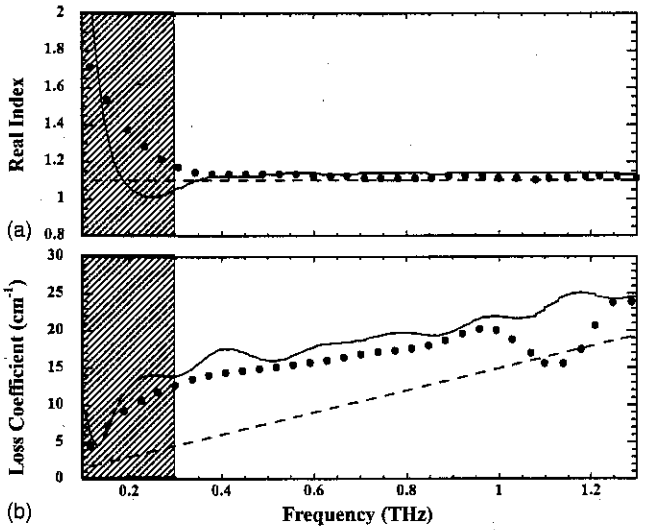

FIG. 3. (a) Comparison of the measured (dots) real part of the effective index, $n_{\mathrm{meas}}(\omega)$, against the calculated $n_{\mathrm{mie}}(\omega)$ for alumina (solid line) and previous frequency independent n_{ind} (dashed line). (b) Comparison of the measured loss coefficient, $\alpha_{\mathrm{meas}}(\omega)$, from the complex effective index against the calculated loss coefficient, $\alpha_{\mathrm{mie}}(\omega)$, and $\alpha_{\mathrm{ind}}(\omega)$ derived from the previously reported frequency independent complex effective index. The measured values are the average for the three signal angles.

of the index shows the wave is weakly coupled to the surface. The loss component, $\alpha_{\mathrm{meas}}(\omega)$, shown in Fig. 3(b) matches Mie theory predictions, $\alpha_{\mathrm{mie}}(\omega)$. However, $\alpha_{\mathrm{meas}}(\omega)$ is consistently higher ($\approx 9\ \mathrm{cm}^{-1}$) than the previously measured loss coefficient. $\alpha_{\mathrm{ind}}(\omega)$, of the surface wave which travels through the cylinder.[8] The lower loss coefficient $\alpha_{\mathrm{ind}}(\omega) = 0.073\,\omega/c$ (with c expressed in cm/s) from the previous work also agrees with Mie theory predictions at $\theta = 13°$ confirming experimental validity, but indicates additional mechanisms are involved with paths crossing interior chords of the target outside the range of the physical optics model. This discrepancy between loss coefficients shows surface waves which cut through the cylinder see an effective enhancement compared to those which do not. The reason for this apparent enhancement is currently not understood, but may be due to other, frequency dependent mechanisms such as coupling into the surface, internal focusing, or diffraction which have not yet been experimentally or theoretically isolated.

This work was partially supported by the National Science Foundation and the Army Research Office.

[1] N. A. Logan, Proc. IEEE **53**, 773 (1965).
[2] H. Uberall and G. Gaunard, Appl. Phys. Lett. **39**, 362 (1981).
[3] H. M. Nussenzveig, J. Math. Phys. **10**, 83 (1969).
[4] R. A. Cheville, R. W. McGowan, and D. Grischkowsky, Phys. Rev. Lett. **80**, 269 (1998).
[5] R. W. McGowan, R. A. Cheville, and D. Grischkowsky, Appl. Phys. Lett. **76**, 670 (2000).
[6] R. A. Cheville and D. Grischkowsky, Appl. Phys. Lett. **67**, 1960 (1995).
[7] R. A. Cheville, R. W. McGowan, and D. Grischkowsky, IEEE Trans. Antennas Propag. **AP-45**, 1518 (1997).
[8] R. W. McGowan, R. A. Cheville, and D. Grischkowsky, IEEE Trans. Microwave Theory Tech. **48**, 417 (2000).